

Temperature modeling of laser-irradiated azo-polymer thin films

Kevin G. Yager and Christopher J. Barrett^{a)}

Department of Chemistry and Centre for the Physics of Materials, McGill University, Montréal, Québec H3A 2K6, Canada

(Received 8 July 2003; accepted 14 October 2003)

Azobenzene polymer thin films exhibit reversible surface mass transport when irradiated with a light intensity and/or polarization gradient, although the exact mechanism remains unknown. In order to address the role of thermal effects in the surface relief grating formation process peculiar to azo polymers, a cellular automaton simulation was developed to model heat flow in thin films undergoing laser irradiation. Typical irradiation intensities of 50 mW/cm² resulted in film temperature rises on the order of 5 K, confirmed experimentally. The temperature gradient between the light maxima and minima was found, however, to stabilize at only 10⁻⁴ K within 2 μ s. These results indicate that thermal effects play a negligible role during inscription, for films of any thickness. Experiments monitoring surface relief grating formation on substrates of different thermal conductivity confirm that inscription is insensitive to film temperature. Further simulations suggest that high-intensity pulsed irradiation leads to destructive temperatures and sample ablation, not to reversible optical mass transport. © 2004 American Institute of Physics.
[DOI: 10.1063/1.1631438]

I. INTRODUCTION

Thin films of polymers containing azobenzene chromophores (azo polymers) have been investigated for over 25 yr as nonlinear optical materials, for liquid crystal alignment, and as photoswitchable materials.¹ In 1995, it was observed that the free surface of azobenzene-polymer films could be induced to exhibit surface mass transport if exposed to a light intensity and/or polarization gradient.^{2,3} The size scale for this process, which essentially encodes the incoming light modulation pattern into a surface relief pattern, is determined by the geometry and the wavelength of light. A typical inscription setup, shown in Fig. 1(a), involves interfering two coherent laser beams at the sample surface. The sinusoidal variation of light results in a sinusoidal surface relief grating (SRG) on the sample free surface, as confirmed by atomic force microscopy [Fig. 1(b)]. The peak-to-peak spacing is typically on the order of hundreds of nanometers, and peak-to-valley amplitudes of hundreds of nanometers are readily obtained with modest irradiation intensities (<50 mW/cm²). This unusual material transport occurs in minutes, and at room temperature, which is well below the bulk glass-to-rubber transition temperature (T_g) for these polymers. The optical inscription is fully reversible, as a flat film of the original thickness is recovered upon heating above T_g . Reviews of the many interesting results are available.^{4,5} The process critically requires a polymer containing azobenzene moieties. Azobenzene and its derivatives undergo photoinduced isomerization between *trans* and *cis* geometries when exposed to light at an absorbing wavelength (Fig. 2). Cycling of chromophores between these isomers appears to be required for the mass transport phenomenon, although the ex-

act role of isomerization is not yet clear. The grating amplitude scales with the net exposure energy up to a saturation point, and therefore scales with irradiation power and time.⁶ The SRG is phase shifted with respect to the incident light pattern, with light intensity maxima corresponding to surface relief minima.⁷ The grating amplitude depends strongly on the polarization combination used in the writing beams, and it has been observed that even a pure polarization pattern can lead to SRG formation.⁸ Mechanisms proposed to explain the mass transport include: isomerization pressure,⁹ gradient electric forces,¹⁰ asymmetric diffusion,¹¹ mean-field forces,¹² and permittivity gradients.¹³ In addition to these mechanisms, the inherent fluid dynamics have been modeled,¹⁴⁻¹⁶ yet the exact nature of the driving force remains unresolved.

Over the course of mechanism investigation, it has generally been assumed that thermal effects do not play a significant role in the inscription process, since inscription is known to depend on the light polarization, yet a purely thermal mechanism would be sensitive only to light intensity. It has recently been suggested, however, that thermal gradients might be responsible for SRG inscription using pulsed irradiation,^{17,18} and it may also be that sample heating is assisting the cw photoinduced mass transport phenomenon. It is therefore of interest to consider quantitatively what effect, if any, thermal gradients may have in pulsed and continuous irradiation experiments. These thermal gradients would be created due to the inhomogeneous illumination of the sample surface, but their magnitude and persistence time would be expected to depend strongly on material parameters, geometry, and size scale. In an effort to understand the role of thermal gradients in the SRG inscription process, we created a straightforward cellular automaton simulation, and used it to predict the temperature gradients for typical inscription conditions. These predictions indicate that thermal gradients are negligible for typical modest irradiations, and

^{a)} Author to whom correspondence should be addressed. Electronic mail: chris.barrett@mcgill.ca

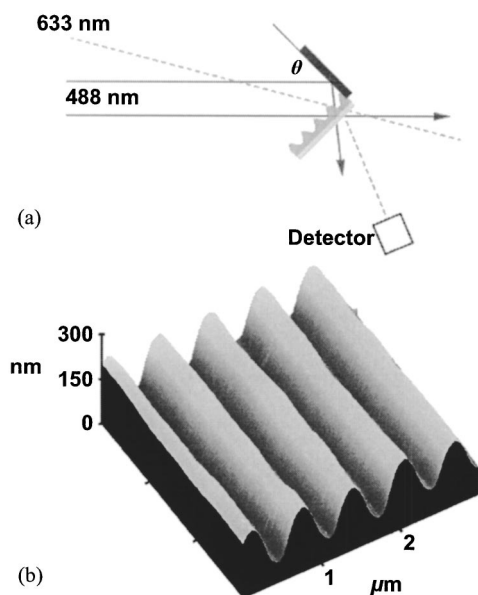


FIG. 1. (a) Typical experimental setup for inscription of surface relief gratings. A 488 nm laser beam is reflected upon itself to generate an interference pattern at the film surface. The resulting diffraction is monitored with a low power HeNe beam (633 nm). (b) AFM image of the resulting surface relief grating. The spacing is determined by the angle θ and the wavelength of light. The grating amplitude depends on many parameters, including light intensity and polarization.

that pulsed irradiations are likely causing destructive sample ablation, and not mass transport. We also present the results of our experimental investigation of SRG formation on substrates of markedly different thermal conductivity (plastic and air), which confirm that the grating mechanism is insensitive to film steady-state temperature. The model presented is general, and should allow estimation of temperature rise in a variety of different experiments and geometries.

II. METHODS

A. Simulation procedure

In order to simulate heat flow in the hundreds of nanometers regime, a rectangular grid of cubic cellular automata

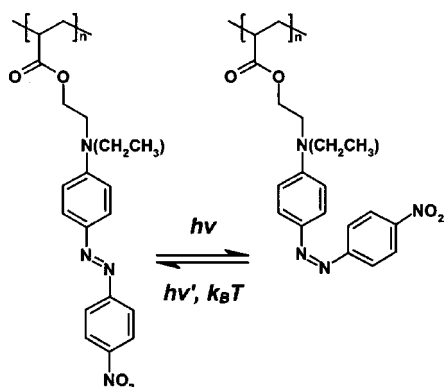


FIG. 2. Azobenzene chromophores isomerize from the *trans* to the *cis* state under irradiation at an absorbing wavelength. The molecule will then thermally relax back to the more stable *trans* state, or this reconversion can be induced photochemically. Depicted above is poly(disperse red 1 acrylate).

was implemented, where diffusive heat energy transfer from cells to nearest neighbors is calculated using the Fourier law

$$J(y,z,t) = -\kappa \left(\frac{\partial T(y,z,t)}{\partial y} \right) - \kappa \left(\frac{\partial T(y,z,t)}{\partial z} \right), \quad (1)$$

where $J(y,z,t)$ is the rate of heat flow at position (y,z) and time t , $T(y,z,t)$ is the temperature, and κ is the thermal conductivity (a material property). The validity of this law for short time and distance scales, with minor deviations from bulk thermal conductivity, has been verified experimentally.¹⁹ The typical SRG inscription experiment can be completely simulated using a two-dimensional slice of material, as shown in Fig. 3. In general, the thin azo film has a free surface (with air above it), and a substrate (such as a glass slide). Approximate bulk material properties for the three layers are shown in Table I.

The optical field is simulated inside the azobenzene film only, with a Beer–Lambert exponential decrease of light intensity in the z direction, and a sinusoidal light variation in the y direction. The left and right hand sides are coupled, forming periodic boundary conditions in the y direction, which correctly describes the periodic oscillation of the light field at the sample surface. The width of the simulation was set to 700 nm, which is approximately the periodicity obtained with 488 nm light interfering at 20°. Simulation in the x direction is not necessary, since no parameters vary along that axis. The top and bottom edges of the simulation rectangle were treated as perfect heat sinks, meaning that any thermal energy in excess of ambient reaching these cells was eliminated. The presence of these heat sinks creates an artifact for any finite simulation size, but as will be discussed later, the results can be interpreted in a way that does not depend on this effect. The results presented here used a vertical simulation size of 10 μm .

Each cell is defined by material properties, specifically thermal conductivity, heat capacity, and extinction coefficient (zero except for the azo film); and by simulation variables, specifically the heat content and temperature at a given time step. The simulation algorithm consists of, on each time step: (1) augmenting the heat energy content of each azobenzene-film cell, based on the calculated light energy absorbed by that cell; (2) calculating the cell temperatures, based upon their current heat content and heat capacity; (3) redistributing energy between nearest neighbors, based on the thermal disparity between the cells and the Fourier law; and (4) resetting the upper and lower boundaries to zero excess heat content. It was found that the simulation results were essentially identical, regardless of the exact choice of cell size and time step duration, so long as these are sufficiently small. For the two-dimensional (2D) simulations presented here, the cells are cubes 10 nm on a side, and the time step is 10^{-12} s, which were determined to be sufficiently small to avoid resolution artifacts. For long simulation times, a simplified one-dimensional (1D) array of cubic cells was instead used, with cell sizes of 100 nm and a timestep of 10^{-10} s. The 1D results shown here were obtained with a 200 μm linear array.

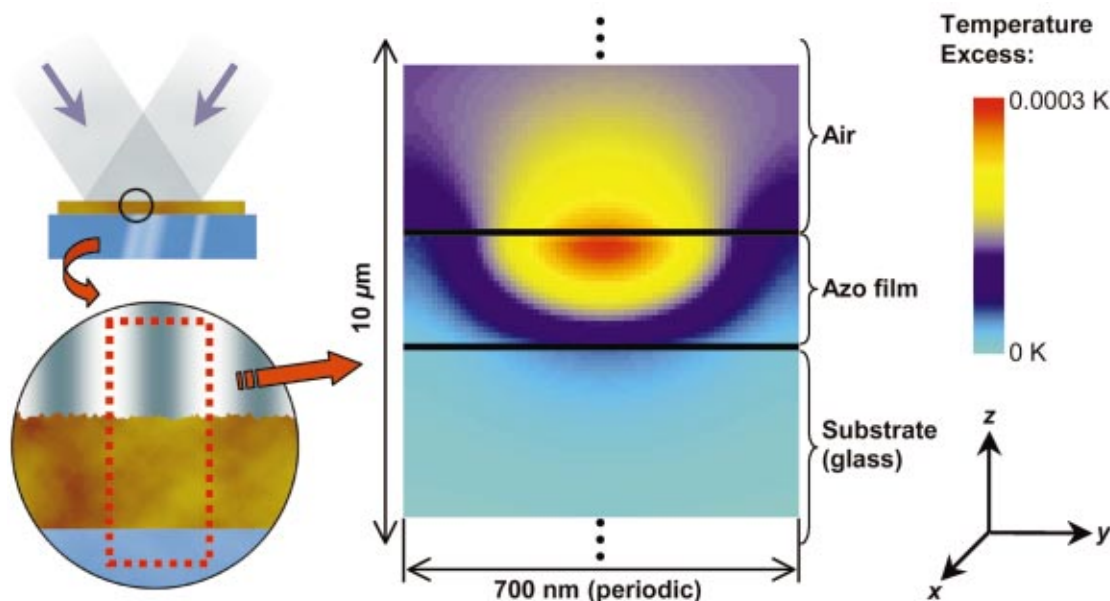


FIG. 3. (Color) Two-dimensional simulation setup. A rectangular simulation region, with periodic boundary conditions, describes a representative section of the azobenzene film. The heat flow calculations predict periodic temperature profiles, as a result of the periodic light pattern at the sample surface. The temperature map shown is the output from a 2D simulation of a 200 nm film, after 10^{-7} s of irradiation with 50 mW/cm^2 .

B. Thin film irradiation

The low molecular weight azobenzene polymer, poly-(disperse red 1 acrylate) (PDR1A), was synthesized as described previously.²⁰ Thin films of PDR1A were spin coated from filtered solutions ($\sim 0.1 \text{ mol/L}$ repeat unit concentration) onto freshly cleaved mica (800 rpm for 35 s, acceleration 1680 rpm/s). The thin film was then floated off onto a water surface, and picked up onto a plastic substrate with an array of 1.5 mm diam holes. Portions of the thin film suspended over the holes are thereby freestanding, and experience an air substrate. The entire film was exposed for one hour to an interference pattern ($\theta = 20^\circ$) from the 488 nm line of an Ar^+ ion laser (Innova 308, Coherent). The beam was circularly polarized, and the power at the sample surface was 10 mW/cm^2 . The resulting SRG, in the areas over the plastic substrate, and over the air substrate, were investigated using atomic force microscopy (BioScope, Digital Instruments). For comparison, a commercially available series of liquid crystal films that exhibit visible color transitions at various temperatures were irradiated with the same laser system.

III. RESULTS AND DISCUSSION

The 2D simulation procedure is inherently limited by available computational power. Thus, to simulate further in the z direction and time, it is necessary to simplify the system somewhat. As will be discussed later, it was found that beyond 10^{-5} s, the heat profile in the y direction had become stabilized. For long simulations, therefore, a simplified 1D array of cells was used. Although the 1D simulation allows access to longer distances and times than the 2D simulation, it is also limited by finite-size artifacts. The simulation results can be compared (at least within order of magnitude) to the analytical result obtained by considering an infinite plane heating a semi-infinite material. For a constant heating rate of w_0 , the temperature profile is²¹

$$T(z,t) = T_i + \frac{2w_0}{\kappa} (\alpha t)^{1/2} \left[\frac{1}{\sqrt{\pi}} e^{-\xi^2} + \xi \operatorname{erf}(\xi) - \xi \right], \quad (2)$$

where erf is the error function, T_i is the initial temperature of the system, $\alpha \equiv \kappa/C$ is the thermal diffusivity, where C is the heat capacity, and

$$\xi = \frac{z}{2\sqrt{\alpha t}}. \quad (3)$$

Of specific interest is the temperature of the plane itself, which is

$$T(0,t) = T_i + \frac{2w_0}{\kappa} \sqrt{\frac{\alpha}{\pi}} t^{1/2}. \quad (4)$$

The analytical solution therefore predicts that the temperature of the thin film should rise as $t^{1/2}$.

The temperatures that will be discussed henceforth are excess temperatures, relative to ambient, since the Fourier

TABLE I. Simulation parameters.

Substance	Heat capacity C (J/Km^3)	Thermal conductivity κ (W/mK)	Thermal diffusivity α (m^2/s)	Extinction coefficient $\epsilon_{488 \text{ nm}}$ (μm^{-1})
Air	1300	0.026	2.3×10^{-5}	0
Azo	1.60×10^6	0.17	1.1×10^{-7}	5.30
Glass	1.56×10^6	0.80	5.1×10^{-7}	0

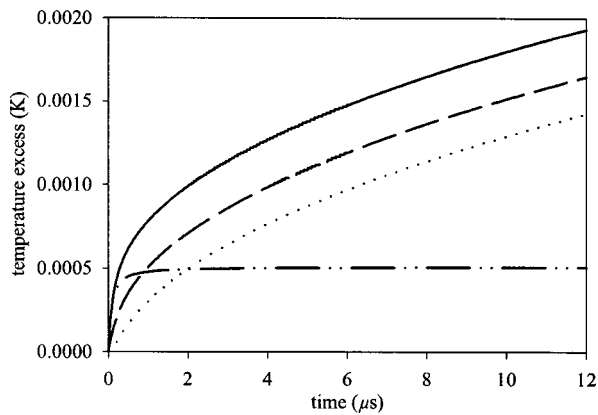


FIG. 4. Typical heat-flow simulation result, in this case for a 200 nm azo film on glass substrate, irradiated with 50 mW/cm² light. The simulation tracks the temperature of the hottest azo cell (solid line), the coldest cell (dotted line), the average of all the azo cells (dashed line), and the temperature difference between the hottest and coldest cells (dot-dashed line).

equation is invariant under uniform temperature offsets. Figure 4 shows a typical simulation output, in this case for a 200 nm azo thin film on a glass substrate, irradiated with 50 mW/cm² of light. The quantities plotted are the temperature of the hottest cell in the azo film, the temperature of the coldest cell, the simple average of all the azo cells, and the difference between the hottest and coldest cells. This temperature difference was invariably found to correspond to the difference between the maximum and minimum of the light irradiation pattern. Any mechanism attempting to explain SRG formation on thermal grounds would presumably be sensitive only to this temperature difference. As can be seen in Fig. 4, the overall temperature of the film continues to rise long after the temperature difference has stabilized. One can approximate a characteristic distance for heat diffusion in time t using \sqrt{at} . Using this relation, one would expect heat flow over a distance of 700 nm to stabilize after $\sim 5 \mu\text{s}$, in agreement with the simulation results. The overall rise in film temperature eventually reaches a steady-state value, which is necessarily dependent upon the finite simulation size. Larger simulations lead to proportional postponement of the finite-size steady-state artifact. The temperature difference curve, however, is found to be invariant under simulation size, and in fact sets in before the finite simulation size plays a role. It therefore seems reasonable to decouple questions regarding the heat flow in the x - y plane and heat flow in the orthogonal z direction. The former relates to the magnitude of thermal gradients inside the film, and the latter to the final absolute temperature of the film.

Longer simulation times become accessible using the 1D cell array, and still longer times using the analytical solution. The 2D, 1D, and analytical approaches are found to superimpose agreeably (Fig. 5). The early portion of the 1D simulation is well described by a curve of the form $T=at^{1/2}$, where the prefactor a is within 10% of the one calculated using Eq. (4) and the parameters for glass. The discrepancy in the values for a , observable at longer time scales, can be entirely attributed to the fact that the simulation incorporates heat loss into the air as well as the glass substrate. Using \sqrt{at} as before, one would expect that after milliseconds, the tem-

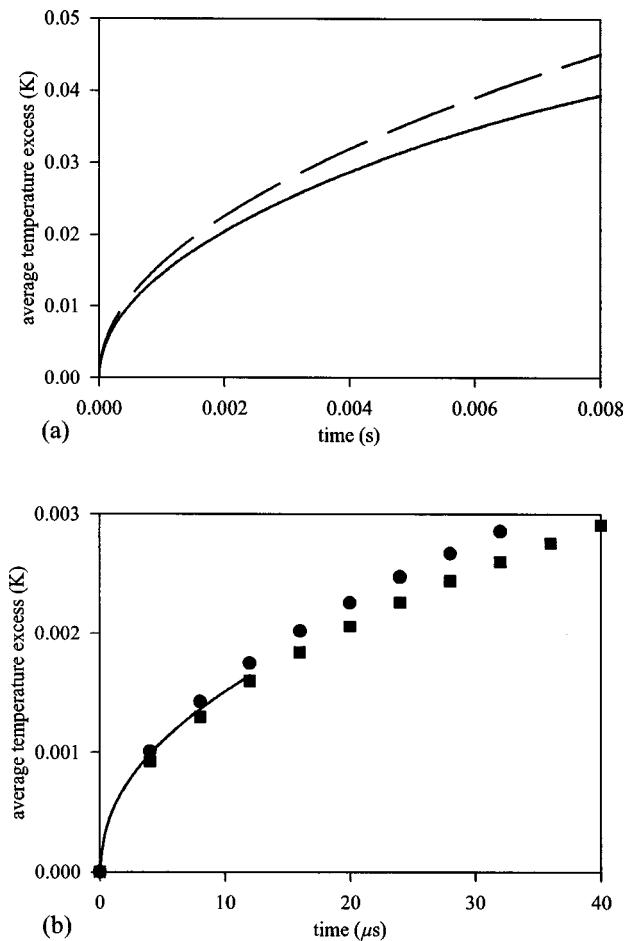


FIG. 5. Comparison of modeling methods, using a 200 nm film under 50 mW/cm² irradiation. (a) The analytical solution (dashed line) is offset slightly from the 1D simulation (solid line) due to different assumptions. (b) The analytical solution (circles), 1D simulation (squares), and 2D simulation (solid line) converge well at short times.

perature profile would reach a steady-state in the z direction. Accordingly, at still longer simulation times, finite-size effects cause the 1D curve to deviate from $T=at^{1/2}$ behavior. The agreement of the three approaches (2D, 1D, analytical) lends strong credibility to the simulation results. Overall, it is predicted that the film temperature rises as $t^{1/2}$ indefinitely. For any realistic macroscopic sample one would eventually have to extend the analysis to include the finite sample size (in the x and y directions) and convective heat flow above the sample. These considerations would necessarily limit the achievable steady-state temperature in a thin film irradiation process. The magnitude and scaling indicate, however, that final film temperatures under modest irradiation will not be very large. Specifically, typical inscription conditions involve irradiating an area approximately 1 cm in size with 50 mW/cm², for minutes. According to Eq. (4), after 5 min of 50 mW/cm² irradiation, the thin film temperature would have risen by ~ 12 K. More realistically, the finite irradiation size would be expected to play a role when the temperature profile in the z direction reaches distances similar to the irradiation size. Using Eq. (3), we predict a substantial (1 K) temperature rise at a distance of 1 cm from the sample after 2 min, at which time the film temperature has risen by 5 K. We

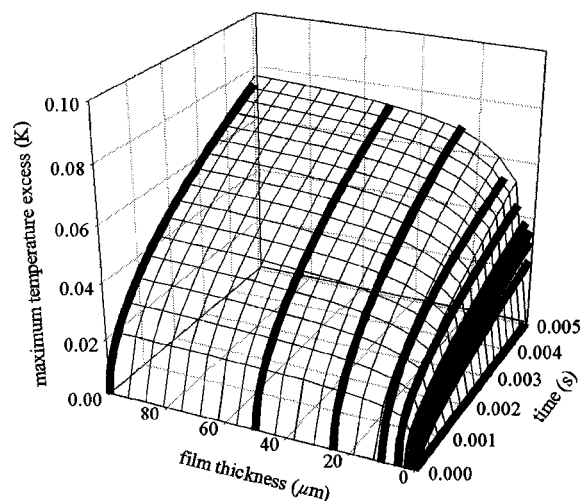


FIG. 6. Scaling of film temperature with film thickness, based on 1D simulation and 50 mW/cm^2 irradiation. The simulation results (thick lines) are well described by a four-parameter fit (mesh). The maximum temperatures achievable saturate to bulk values for films greater than $50 \mu\text{m}$. The $t^{1/2}$ dependence is satisfied for all film thickness values.

expect final film temperatures to be on the order of $\sim 5 \text{ K}$ above ambient, which is consistent with the measured temperature rise in a thin azobenzene polymer film under 100 mW/cm^2 irradiation.²² We performed a further verification experiment, by irradiating a series of liquid crystal films that exhibit visible color transitions at different temperatures, and found that irradiation with 20 mW/cm^2 caused a $\sim 7 \text{ K}$ temperature rise, and irradiation with 50 mW/cm^2 caused a $\sim 10 \text{ K}$ temperature rise. More importantly, the simulations indicate that any thermal gradient will be very small, stabilizing at $\sim 5 \times 10^{-4} \text{ K}$ after $2 \mu\text{s}$. It is unlikely that such a small thermal contrast would lead to any interesting spatial variation of material properties. Thermal gradient mechanisms at modest irradiation are therefore effectively ruled out by these results.

A. Effect of film thickness

As film thickness is increased, the fraction of incoming light that is absorbed increases, which leads to an overall increase in the film heat energy content. The very bottom of thicker films, however, sees proportionally less irradiance as the thickness is increased, so that the minimum temperature becomes proportionally lower. The maximum film temperature increases as the film thickness is increased, corresponding to trapping of heat at the sample surface, but this effect eventually saturates to a bulk value (Fig. 6). The saturation of the film thickness effect can be fit to, for example, a rectangular hyperbolic function. The entire simulation data set, as a function of time t and thickness h is well described by an equation of the form

$$T_{\max}(t, h) = \left[\frac{bh}{c+h} + \frac{dh}{e+h} \right] t^{1/2}, \quad (5)$$

where b through e are fitting parameters, and the term in square brackets is essentially the parameter a . Thus, we can

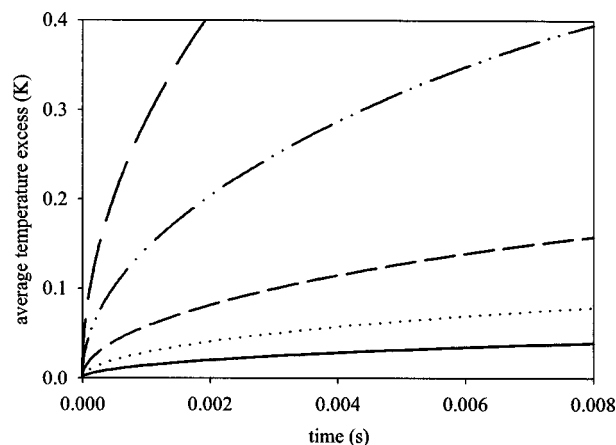


FIG. 7. Predicted 1D simulation scaling of the temperature in a 200 nm with irradiation power: 50 mW/cm^2 (solid line), 100 mW/cm^2 (dotted line), 200 mW/cm^2 (short dashes), 500 mW/cm^2 (dot-dashed line), 1000 mW/cm^2 (long dashes).

set an upper bound on the temperature rise even in a bulk-like material. This final temperature excess is small even for the thickest films.

B. Effect of laser power

In agreement with the analytical prediction, Eq. (4), laser power causes a linear scaling of temperature. Laser irradiances above 1 W/cm^2 , known experimentally to photodegrade azo materials, lead to significant temperature rises. From Eq. (3), irradiation with 1 W/cm^2 leads to a 1 K rise at 1 cm from the film in less than 30 s , at which time the film temperature has increased by 50 K . High laser power densities are known to cause photobleaching by breaking the azo bond. It is possible that photo-induced heating above the material's degradation temperature of 180°C contributes to sample damage under intense laser light. This prediction is the same order of magnitude as the 15 K temperature rise measured in a thin film polymer light-emitting diode (LED) subjected to 1 W/cm^2 of power input.²³ The agreement is more quantitative when one adjusts for the small size (4 mm^2) of the LED active area compared to the laser spot sizes ($\sim 1 \text{ cm}^2$) being considered here. These results also agree with the observed reduction in softening temperature for an azobenzene thin film under 2.4 W/cm^2 laser light illumination, which indirectly suggested a $\sim 12 \text{ K}$ photoheating effect.²⁴ It has been observed that using high laser power, greater than 20 W/cm^2 , an in-phase SRG is superimposed upon the out-of-phase SRG obtained under low power irradiation.⁶ The in-phase grating cannot be photoerased, suggesting an irreversible, destructive mechanism. The postulation that this second SRG results from thermal degradation or crosslinking is supported by the present simulations, which predict substantial temperature rises, well above T_g and the degradation temperature (see Fig. 7).

C. Effect of substrate (thermal conductivity)

Equation (4) predicts a ~ 200 -fold difference in film temperatures between the case of glass and air substrates, owing to the markedly different thermal conductivities and

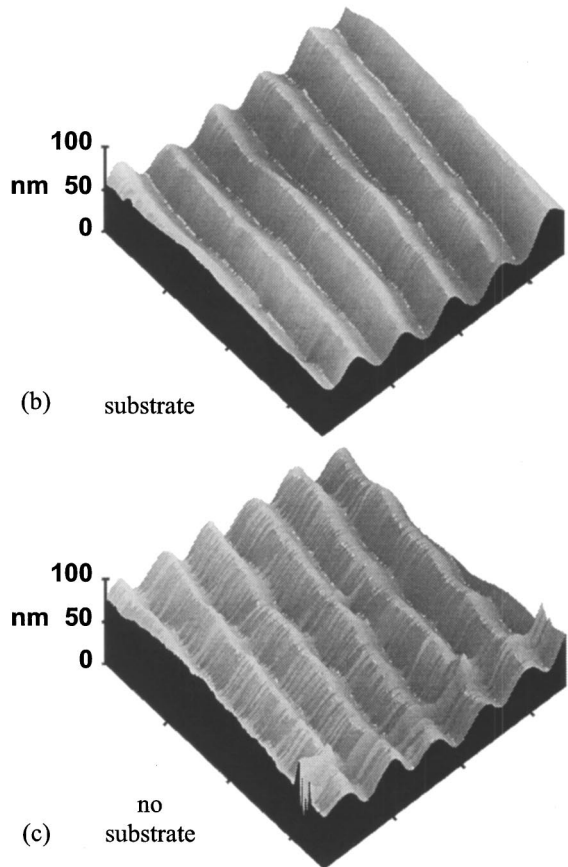
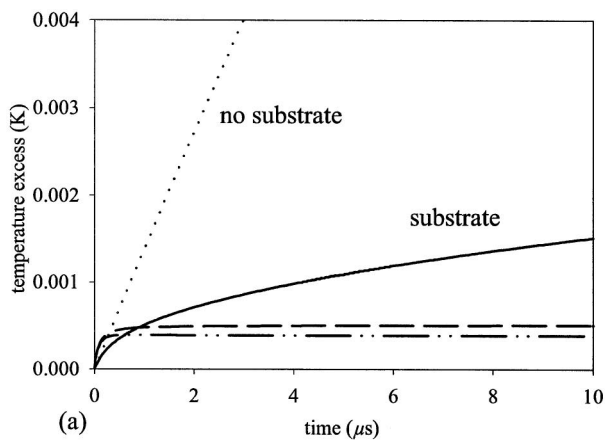


FIG. 8. (a) Two-dimensional simulation of temperature excess for irradiation (50 mW/cm^2) of a thin film (200 nm) on a glass substrate vs air substrate. The average film temperature for glass substrate (solid line) is much smaller than for air substrate (dotted line), whereas the temperature difference for glass substrates (dashed line) and air substrates (dot-dashed line) is identical. There is no experimental difference between the SRG obtained on a plastic substrate (b) vs air substrate (c).

heat capacities. Simulation results suggest that the absolute temperature rise of the film will be at least one order of magnitude higher when it is suspended over a good insulator such as air. The lateral temperature difference, however, is not affected by substrate thermal conductivity [Fig. 8(a)]. In order to experimentally investigate substrate effects, a free-standing polymer film was deposited onto a plastic substrate with holes. The areas of the film on the plastic substrate experience much better thermal conduction (approximately equal to the glass substrate considered in the simulations)

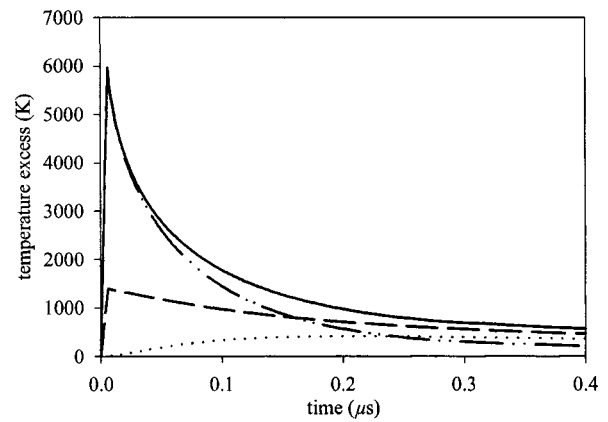


FIG. 9. Temperature rise predicted by the 2D simulation for a 6 ns laser pulse of total energy 50 mJ/cm^2 . The hottest cell (solid line) reaches nearly 6000 K after 6 ns , whereas the coldest cell (dotted line) reaches its maximum temperature after the pulse. The average temperature (dashed line) and temperature difference (dot-dashed line) indicate that extremely high temperatures are achieved under pulsed irradiation.

than the areas suspended over the holes, which experience an air substrate. The atomic force microscope (AFM) images of SRG inscription in the two areas are shown in Figs. 8(b) and 8(c). Despite the significantly different film temperatures in the two regions, the SRG's are essentially identical. Any photothermal effects at play in surface relief inscription are too weak to be observed in this experiment. There is mounting evidence for a photoinduced material softening in azobenzene thin films,^{10,24–26} but these simulation results indicate that it has a negligible thermal component.

D. Pulsed irradiation

A pulsed irradiation was simulated by using a square-wave light pulse. The photoenergy input was set to be $8.3 \times 10^6 \text{ W/cm}^2$ for 6 ns , corresponding to 50 mJ/cm^2 of energy. The result can be seen in Fig. 9, where the film temperature rises sharply and nearly linearly for the duration of the pulse. After the pulse, the film cools and redistributes thermal energy. The hottest cells in the film experience a temperature rise of nearly 6000 K during the pulse, well beyond the typical damage threshold ($\sim 180^\circ\text{C}$) for these materials. In the polymer photoablation literature, temperature increases on the order of 10^3 K have been reported for strongly absorbing samples.^{27–30} It therefore seems likely that pulsed experiments on azobenzene polymer thin films are generating thermal gradients of sufficient magnitude in order to destroy the sample. This is contrary to the postulation that thermal gradients lead to spatial variation of material properties (such as the permittivity), and thereby to optical forces.¹⁸ The foregoing analysis has, however, not included many pertinent effects, such as the nonlinear absorption of the azobenzene chromophores at high laser field intensity, and the temperature dependence of the material properties shown in Table I. It should also be noted that if ablation is occurring, then the film geometry is changing with time, which the simulation ignores. The simulation nevertheless gives an order of magnitude estimate of sample

heating, and strongly suggests that laser pulses are causing material ablation that is in no way unique to azobenzene chromophores.

To verify the pulsed irradiation simulation, we solved analytically for the temperature distribution. Over the course of a 6 ns pulse, the characteristic distance for heat diffusion is $\sqrt{\alpha t} \approx 25$ nm. Given this short distance, the pulsed experiments can be considered in two parts: an irradiation phase where diffusion is neglected, and a diffusion phase after energy input has ceased. The temperature rise at time t during the pulse, assuming no diffusion, can be written

$$T(y, z, t) = \frac{I_0 t \varepsilon \ln 10}{C} \left[2 \sin^2 \left(\frac{\pi}{\Lambda} y \right) 10^{-\varepsilon(h-z)} \right], \quad (6)$$

where I_0 is the incident irradiation intensity, ε is the material extinction coefficient, h is the film thickness, and Λ is the spacing of the interference pattern (700 nm for the configurations considered here). The term in square brackets denotes

the light distribution pattern inside the film. Using Eq. (6), one predicts a ~ 7600 K increase for the hottest point in the film at the end of the pulse, which is within 20% of the result shown in Fig. 9. The average temperature can be computed as

$$T_{\text{avg}} = \frac{\int_0^h \int_0^\Lambda T(y, z, t) dy dz}{\int_0^h \int_0^\Lambda dy dz} = \frac{I_0 t}{hC} [1 - 10^{-\varepsilon h}]. \quad (7)$$

Using the same parameters as for Fig. 9, this equation predicts an average film temperature of ~ 1400 K at the end of the pulse, which is within 2% of the simulation result. The heat diffusion phase can be analyzed by decomposing the temperature distribution that results from the laser pulse into a spatial distribution of instantaneous point heat sources³¹

$$T(y, z, t) = \frac{Q}{8(\pi\alpha t)^{3/2}} \int_{-\infty}^{\infty} d\bar{x} \int_{-\infty}^{\infty} d\bar{y} \int_0^h d\bar{z} \exp\left(-\frac{(x-\bar{x})^2 + (y-\bar{y})^2 + (z-\bar{z})^2}{4\alpha t}\right) \left[2 \sin^2\left(\frac{\pi}{\Lambda}\bar{y}\right) 10^{-\varepsilon(h-\bar{z})} \right] \\ = \frac{Q}{2\pi\alpha t} \int_{-\infty}^{\infty} \exp\left(-\frac{(y-\bar{y})^2}{4\alpha t}\right) \sin^2\left(\frac{\pi}{\Lambda}\bar{y}\right) d\bar{y} \int_0^h \exp\left(-\frac{(z-\bar{z})^2}{4\alpha t} - \varepsilon \ln 10(h-\bar{z})\right) d\bar{z}, \quad (8)$$

where the time t now refers to time after the pulse, since the pulse duration is assumed to be negligibly small. Equation (8) can subsequently be used as a solution to the heat diffusion law, and the temperature profile during the pulse can be recomputed more rigorously.³²

Equation (8) has implicitly assumed that α is the same everywhere. That is, only a single infinite material is considered. When this equation is compared with a simulation using the same assumption (identical thermal properties in the three regions), the agreement is very good, at all times. At long times ($> 10^{-7}$ s), the simulation and analytic results agree to within 2% or better. Near $t=0$ s (i.e., immediately after the pulse), the agreement is between 1% and 15%, depending on the location inside the film. In addition to further validating the simulation procedure presented in this paper, the comparison with analytic results confirms that azo films under pulsed irradiation are likely to achieve temperatures rises of several thousand Kelvin.

IV. CONCLUSION

The thermal model developed here for irradiated thin films is simple and robust, appearing to yield reasonable order-of-magnitude estimates for typical situations. Clearly this technique could be extended to other cases, such as consideration of thermal effects in light propagation down a narrow fiber-optic, NSOM tip, or slab waveguide. With respect to the surface relief inscription process unique to azobenzene polymers, these simulations strongly indicate that thermal effects do not play any appreciable role. Specifically, the

overall temperature change under modest irradiation is too small to lead to a change of material properties or softening of the sample. The temperature gradient achieved within the sample is on the order of 10^{-4} K, and does not appear to vary with inscription or geometric conditions. This gradient cannot lead to an appreciable spatial variation of material properties, and certainly does not explain the dependence of SRG inscription on many variables. Surface relief gratings formed under markedly different thermal conditions were essentially identical, further discounting the role of thermal effects. Although there is mounting evidence that azobenzene photoisomerization leads to material softening, it now seems unlikely that there is an appreciable thermal component. The simulations performed here suggest that pulsed irradiation leads to destructive sample ablation, a well-established phenomenon in strongly absorbing polymer systems, rather than to reversible optical mass transport. Thermal effects in small systems can depend sensitively on many parameters, but it appears that even simple cellular automata, as presented here, can capture much of the behavior at a meso scale in a reasonable way.

ACKNOWLEDGMENTS

Funding for this project was provided by NSERC Canada in the form of grants (C.B.) and scholarships (K.Y.), by FCAR Quebec in the form of scholarships (K.Y.), and by the Canadian Foundation for Innovation. The authors are grateful to Nasir Ahmad for materials synthesis, and to Peter Grütter for instrument time.

- ¹S. Xie, A. Natansohn, and P. Rochon, *Chem. Mater.* **5**, 403 (1993).
- ²P. Rochon, E. Batalla, and A. Natansohn, *Appl. Phys. Lett.* **66**, 136 (1995).
- ³D. Y. Kim, S. K. Tripathy, L. Li, and J. Kumar, *Appl. Phys. Lett.* **66**, 1166 (1995).
- ⁴N. K. Viswanathan, D. Y. Kim, S. P. Bian, J. Williams, W. Liu, L. Li, L. Samuelson, J. Kumar, and S. K. Tripathy, *J. Mater. Chem.* **9**, 1941 (1999).
- ⁵K. G. Yager and C. J. Barrett, *Curr. Opin. Solid State Mater. Sci.* **5**, 487 (2001).
- ⁶S. Bian, J. M. Williams, D. Y. Kim, L. Li, S. Balasubramanian, J. Kumar, and S. Tripathy, *J. Appl. Phys.* **86**, 4498 (1999).
- ⁷S. Bian, L. Li, J. Kumar, D. Y. Kim, J. Williams, and S. K. Tripathy, *Appl. Phys. Lett.* **73**, 1817 (1998).
- ⁸N. K. Viswanathan, S. Balasubramanian, L. Li, S. K. Tripathy, and J. Kumar, *Jpn. J. Appl. Phys., Part 1* **38**, 5928 (1999).
- ⁹C. J. Barrett, A. L. Natansohn, and P. Rochon, *J. Phys. Chem.* **100**, 8836 (1996).
- ¹⁰J. Kumar, L. Li, X. L. Jiang, D. Y. Kim, T. S. Lee, and S. Tripathy, *Appl. Phys. Lett.* **72**, 2096 (1998).
- ¹¹P. Lefin, C. Fiorini, and J. M. Nunzi, *Pure Appl. Opt.* **7**, 71 (1998).
- ¹²T. G. Pedersen, P. M. Johansen, N. C. R. Holme, P. S. Ramanujam, and S. Hvilsted, *Phys. Rev. Lett.* **80**, 89 (1998).
- ¹³O. Baldus and S. J. Zilker, *Appl. Phys. B: Lasers Opt.* **72**, 425 (2001).
- ¹⁴C. J. Barrett, P. L. Rochon, and A. L. Natansohn, *J. Chem. Phys.* **109**, 1505 (1998).
- ¹⁵K. Sumaru, T. Yamanaka, T. Fukuda, and H. Matsuda, *Appl. Phys. Lett.* **75**, 1878 (1999).
- ¹⁶D. Bublitz, B. Fleck, and L. Wenke, *Appl. Phys. B: Lasers Opt.* **72**, 931 (2001).
- ¹⁷A. Leopold, J. Wolff, O. Baldus, M. R. Huber, T. Bieringer, and S. J. Zilker, *J. Chem. Phys.* **113**, 833 (2000).
- ¹⁸O. Baldus, A. Leopold, R. Hagen, T. Bieringer, and S. J. Zilker, *J. Chem. Phys.* **114**, 1344 (2001).
- ¹⁹N. Taketoshi, T. Baba, and A. Onu, *Jpn. J. Appl. Phys., Part 2* **38**, L1268 (1999).
- ²⁰A. Natansohn, P. Rochon, J. Gosselin, and S. Xie, *Macromolecules* **25**, 2268 (1992).
- ²¹J. M. Hill and J. N. Dewynne, *Heat Conduction* (Blackwell Scientific, Boston, 1987), p. 84.
- ²²S. Bauer-Gogonea, S. Bauer, W. Wirges, and R. Gerhard-Multhaupt, *J. Appl. Phys.* **76**, 2627 (1994).
- ²³J. M. Lupton, *Appl. Phys. Lett.* **80**, 186 (2002).
- ²⁴N. Mechau, D. Neher, V. Börger, H. Menzel, and K. Urayama, *Appl. Phys. Lett.* **81**, 4715 (2002).
- ²⁵T. Srihirin, A. Laschitsch, D. Neher, and D. Johannsmann, *Appl. Phys. Lett.* **77**, 963 (2000).
- ²⁶M. Kameda, K. Sumaru, T. Kanamori, and T. Shinbo, *J. Appl. Polym. Sci.* **88**, 2068 (2003).
- ²⁷P. E. Dyer and J. Sidhu, *J. Appl. Phys.* **57**, 1420 (1985).
- ²⁸G. Gorodetsky, T. G. Kazyaka, R. L. Melcher, and R. Srinivasan, *Appl. Phys. Lett.* **46**, 828 (1985).
- ²⁹B. Danielzik, N. Fabricius, M. Röwekamp, and D. von der Linde, *Appl. Phys. Lett.* **48**, 212 (1986).
- ³⁰D. Dijkkamp, A. S. Gozdz, T. Venkatesan, and X. D. Wu, *Phys. Rev. Lett.* **58**, 2142 (1987).
- ³¹H. S. Carslaw and J. C. Jaeger, *Conduction of Heat in Solids* (Oxford University Press, London, 1986), p. 255.
- ³²K. Brugger, *J. Appl. Phys.* **43**, 577 (1972).